Published in IET Microwaves, Antennas & Propagation
Received on 13th May 2008
Revised on 9th December 2008
doi: 10.1049/iet-map.2008.0171

ISSN 1751-8725

Omnidirectional ADE antenna with a GO-shaped main reflector for an arbitrary far-field pattern in the elevation plane

J.R. Bergmann[1] *F.J.S. Moreira*[2]

[1]*Center for Telecommunications Studies of the Pontifical Catholic University of Rio de Janeiro, Rio de Janeiro, RJ 22453-900, Brazil*
[2]*Department of Electronics Engineering of the Federal University of Minas Gerais, Belo Horizonte, MG 30161-970, Brazil*
E-mail: bergmann@cetuc.puc-rio.br

Abstract: This work presents a formulation for shaping the main reflector of a dual-reflector antenna designed to offer an omnidirectional coverage with an arbitrary radiation pattern in the vertical plane. The subreflector is generated by an axis-displaced ellipse and the main reflector is shaped to achieve a prescribed far-field radiation pattern. The shaping procedure is based on geometrical optics (GO) principles. Two distinct far-field ray structures are investigated. The GO-shaping results are validated by an analysis using the accurate method of moments technique.

1 Introduction

Broadband wireless access systems, like WiMAX and LMDS, have been considered for 'last mile' connectivity at high data rates, providing services of video, voice and data [1, 2]. These systems are based on the cellular radio concept, where base-station antennas are required to provide uniform coverage in the azimuthal plane. This can be achieved either with an omnidirectional antenna at the centre of the cell or with a set of sectorial-coverage antennas [3–10]. For communications at microwave and millimetre-wave bands, some attention has been devoted to reflector systems yielding omnidirectional coverage [5–11]. These omnidirectional antenna designs are especially attractive because of their inherently broadband characteristics and can be used as hub-station radiators for point-to-multipoint radio links. They use circularly symmetric surfaces generated either by conic sections or by sections shaped to control the radiation pattern in the elevation plane.

Among the shaped reflector examples, single- and dual-reflector configurations have been designed to generate cosecant square radiation patterns in the elevation plane [6, 8, 10, 11]. Although simpler, the single-reflector geometry requires a diameter that is larger than those of the dual-reflector antenna and, consequently, does not yield a compact arrangement, as discussed in [9]. The dual-reflector designs of [6, 8] radiate a vertically polarised field by using a TM_{01} conical horn to illuminate a parabolic subreflector, which redirects the energy towards a shaped main reflector that can be either concave or convex, depending on the kind of ray structure (with real or virtual caustic) that emerges from the main reflector towards the far-field region. However, the use of a parabolic subreflector in the dual-reflector configurations presented in [6–9] has the disadvantage of increasing the antenna return loss, as part of the energy incident on the subreflector is redirected towards the horn's aperture. To reduce this drawback, in [12–14] the use of omnidirectional axis-displaced confocal conics generating a virtual or a real annular caustic between the reflectors, according to the different types of geometries, is suggested. Besides the control of the return loss, they bring additional variables to the antenna problem, allowing the designer to achieve higher performances and even more compact geometries [13, 14].

In this work, we present a simple and efficient shaping procedure for omnidirectional dual-reflector antennas based on geometrical optics (GO) principles. To minimise the antenna return loss, the dual-reflector configuration – based on the omnidirectional axis-displaced ellipse (OADE)

antenna of [12–14] – uses an axis-displaced ellipse as a subreflector and a GO-shaped main reflector to control the radiation pattern in the elevation plane. To ensure vertical polarisation, the dual-reflector antenna designs are fed by the coaxial TEM horn described in [10]. In Section 2, some geometrical features of the present omnidirectional dual-reflector configurations are briefly discussed. In Section 3, close-form design equations for the subreflector are presented in terms of pertinent input parameters. In Section 4, the GO main-reflector shaping algorithm, which is based on [10, 15], is derived. In Section 5, two studies of OADE configurations, shaped to generate a cosecant square radiation pattern in the elevation plane, are investigated. All case studies discussed in Section 5 are validated by analyses based on the method of moments (MoM) technique, which accounts for all electromagnetic effects present on the reflector and feed structure [16–18]. This work finally presents some brief conclusions.

2 Basic OADE geometrical features

The OADE antenna is composed of two circularly symmetric reflectors with a common symmetry axis (z-axis), as illustrated in Fig. 1. Most of its geometrical features are extensively discussed in [12–14]. The subreflector is generated by an axis-displaced ellipse and has its vertex (point Q) at the symmetry axis, where a curvature discontinuity is generally present. The foci of the generating ellipse are at the origin of the coordinate system (point O) and at point $P(\rho_P, z_P)$, which has cylindrical coordinates

$$\begin{aligned} \rho_P &= 2c \sin\beta \\ z_P &= 2c \cos\beta \end{aligned} \tag{1}$$

where β is the tilt angle of the ellipse axis and $2c$ is the ellipse inter-focal distance (see Fig. 1). After the rotation around the symmetry axis, P generates an annular caustic and a spherical wavefront emerging from O (where the feed phase centre should be placed) will be reflected by the subreflector as an astigmatic wavefront propagating towards the real annular caustic P.

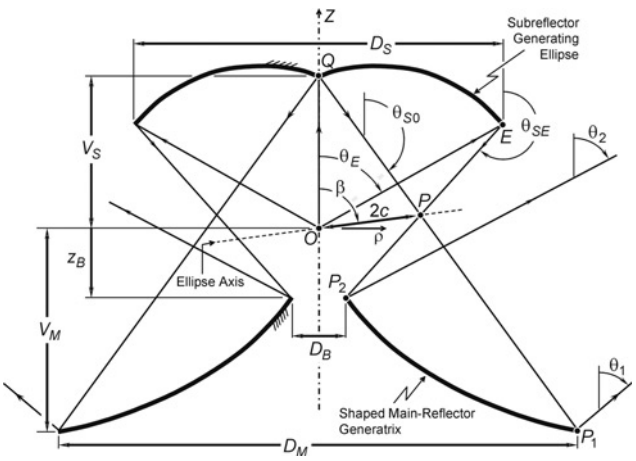

Figure 1 *Basic parameters of the OADE antenna with a shaped main reflector*

The (shaped) main-reflector generatrix is limited by points P_1 and P_2, which define the main-reflector outer and inner edges, respectively. P_2 should be appropriately placed out of the symmetry axis to allow feed access to the principal focus O. By applying GO principles, the main-reflector generatrix will be shaped to reflect the rays coming from the annular caustic P towards the far-field region to obtain a specified radiation pattern in the elevation plane.

The dual-reflector system is illuminated by a feed with a phase centre at O and a circularly symmetric radiation pattern $G_F(\theta_F)$, where θ_F is the angle of the feed ray with the z-axis. A (assumed) spherical wavefront emerging from O will be transformed into a spherical wavefront at the OADE far-field region with a corresponding radiation pattern $G_A(\theta)$, where θ is the angle of observation with the z-axis. According to GO principles, the transformation $G_F(\theta_F) \rightarrow G_A(\theta)$ can be achieved by two different ray structures – emerging from the main reflector and directed towards the far-field region, as illustrated in Fig. 2. Such ray structures differ from each other in the location of the main-reflector caustic, which can be virtual or real, as depicted in Figs. 2a and 2b, respectively. Consequently, they will lead to different main-reflector shapes and dimensions.

3 Subreflector design

The generatix of the subreflector is an axis-displaced ellipse with eccentricity ε, inter-focal distance $2c$ and axial tilt angle β, as illustrated in Fig. 1. From the polar equation of the conic section and with the help of the formulation presented in [15], one can show that the subreflector generating ellipse can be described by the position vector

$$\vec{r}_S(\theta_F) = \frac{c(\varepsilon^2-1)\left[2\eta_F\hat{\rho} + (\eta_F^2-1)\hat{z}\right]}{\varepsilon\left[(\varepsilon\cos\beta-1)\eta_F^2 + 2\eta_F\varepsilon\sin\beta - (\varepsilon\cos\beta+1)\right]} \tag{2}$$

where $\hat{\rho}$ and $\hat{z}$ are the usual cylindrical unit directions and

$$\eta_F = \cot\left(\frac{\theta_F}{2}\right) \tag{3}$$

From [15] one can also obtain a useful relation between the angle θ_F of the incident feed ray and the angle θ_S of the corresponding ray reflected by the subreflector (see Fig. 2):

$$\eta_S = \cot\left(\frac{\theta_S}{2}\right) = \frac{(\varepsilon\cos\beta+1) - \eta_F\varepsilon\sin\beta}{\varepsilon\sin\beta + (\varepsilon\cos\beta-1)\eta_F} \tag{4}$$

The subreflector surface is uniquely specified by the three parameters of the generating ellipse (ε, $2c$ and β) and the subreflector edge angle θ_E (see Fig. 1). However, for practical

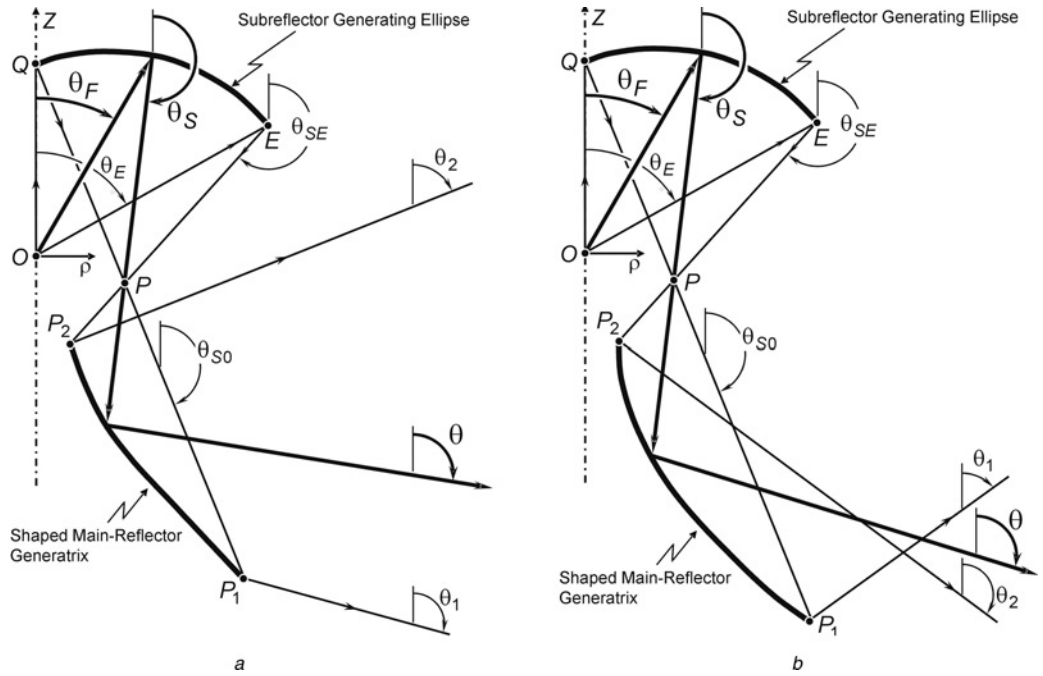

Figure 2 *Ray structures for the OADE with a shaped main reflector*
a With virtual main-reflector caustic
b With real main-reflector caustic

designs, it is more appropriate to specify the subreflector by dimensions, like the subreflector-projected diameter D_S and the distance V_S between the feed phase centre (O) and the subreflector vertex (Q). Another interesting input parameter is the diameter D_B of the main-reflector central opening (see Fig. 1), which must be large enough to enable the feed access to the principal focus without compromising the compactness the main reflector. Furthermore, it is anticipated that the main-reflector shaping departs from a fixed point P_2. Thus, the z-coordinate of P_2 (z_B, depicted in Fig. 1) is also established a priori.

The conic parameters ε, $2c$ and β can be obtained from θ_E, D_S, V_S, D_B and z_B as follows: with the help of Figs. 1 and 2, one can always show from (2) that

$$\left|\vec{r}_S(\theta_F = 0)\right| = V_S = \frac{c(\varepsilon^2 - 1)}{\varepsilon(\varepsilon \cos \beta - 1)} \tag{5}$$

Then, from (2) and (5) one can obtain the following relation:

$$\begin{aligned} D_S &= 2\left|\vec{r}_S(\theta_F = \theta_E)\right| \sin \theta_E \\ &= \frac{4V_S(\varepsilon \cos \beta - 1)\eta_E}{(\varepsilon \cos \beta - 1)\eta_E^2 + 2\eta_E \varepsilon \sin \beta - (\varepsilon \cos \beta + 1)} \end{aligned} \tag{6}$$

where

$$\eta_E = \cot\left(\frac{\theta_E}{2}\right) \tag{7}$$

From (4)

$$\eta_{SE} = \cot\left(\frac{\theta_{SE}}{2}\right) = \frac{(\varepsilon \cos \beta + 1) - \eta_E \varepsilon \sin \beta}{\varepsilon \sin \beta + (\varepsilon \cos \beta - 1)\eta_E} \tag{8}$$

which, together with (6), provides expressions for ε and β

$$\varepsilon \sin \beta = \frac{2\eta_E\left[D_S(\eta_E - \eta_{SE}) - 4V_S\right]}{D_S(1 + \eta_E^2)(\eta_E - \eta_{SE}) - 4V_S\eta_E(\eta_E + \eta_{SE})} \tag{9}$$

$$\varepsilon \cos \beta = \frac{D_S(-1 + \eta_E^2)(\eta_E - \eta_{SE}) - 4V_S\eta_E(\eta_E + \eta_{SE})}{D_S(1 + \eta_E^2)(\eta_E - \eta_{SE}) - 4V_S\eta_E(\eta_E + \eta_{SE})} \tag{10}$$

The value of η_{SE} necessary to evaluate (9) and (10) can be obtained with the help of Fig. 1

$$\cot \theta_{SE} = \frac{\eta_{SE}^2 - 1}{\eta_{SE}} = \frac{2\left[(D_S/2)\cot \theta_E - z_B\right]}{D_S - D_B} \tag{11}$$

which can be rewritten as

$$\eta_{SE} = \left(\frac{D_S \cot \theta_E - 2z_B}{D_S - D_B}\right) - \delta\sqrt{\left(\frac{D_S \cot \theta_E - 2z_B}{D_S - D_B}\right)^2 + 1} \tag{12}$$

where $\delta = +1$ or -1 for $D_S > D_B$ or $D_S < D_B$, respectively. Once ε and β are obtained from the solution of (9) and (10), c can be readily calculated from (5).

doi: 10.1049/iet-map.2008.0171

4 Main-reflector shaping

Many GO reflector-shaping algorithms have been developed since Galindo's pioneering works [19]. For the task at hand, we have adopted a procedure based on [15], which was originally proposed for the GO shaping of offset single reflectors. The procedure has been appropriately adapted for the main-reflector shaping of circularly symmetric dual-reflector antennas in order to obtain a specified far-field radiation pattern in the elevation plane.

Following [15], let the main reflector be represented by a real function $L(\eta_S)$, such that a point at this surface is located by the position vector

$$\vec{r}_{\mathrm{M}}(\theta_{\mathrm{S}}) = \left[\rho_P + 2\eta_{\mathrm{S}} e^{L(\eta_{\mathrm{S}})}\right]\hat{\rho} + \left[z_P + (\eta_{\mathrm{S}}^2 - 1)e^{L(\eta \mathrm{S})}\right]\hat{z} \tag{13}$$

where ρ_P and z_P are the cylindrical coordinates of P given by (1). From the law of reflection, the relation between the incident and the reflected directions – conveniently represented by $\eta_{\mathrm{S}} = \cot(\theta_{\mathrm{S}}/2)$ and $\eta = \cot(\theta/2)$, respectively – at the main-reflector surface is given by [15]

$$\frac{\partial L(\eta_{\mathrm{S}})}{\partial \eta_{\mathrm{S}}} = \frac{2}{\eta - \eta_{\mathrm{S}}} \tag{14}$$

Equation (14) differs from that of [15] by a factor 2 because, due to the present circular symmetry, there is no azimuthal (ϕ) variation. Consequently, η_{S} and $L(\eta_{\mathrm{S}})$ are real valued and the derivative of the former is given by (14).

The main-reflector synthesis consists in finding $L(\eta_{\mathrm{S}})$ from the numerical integration of (14) to describe the surface with (13). The evaluation of (14) can be performed in terms of θ_{F}, which is varied from 0 to θ_{E} to span the main-reflector generatrix. On doing so, η_{S} varies from η_{S0}, which is the value of η_{S} for $\theta_{\mathrm{F}} = 0$, to η_{SE}, given by (12). From (4), (9) and (10), one obtains

$$\eta_{\mathrm{S0}} = \cot\left(\frac{\theta_{\mathrm{S0}}}{2}\right) = \frac{\eta_{\mathrm{E}}\left[D_{\mathrm{S}}(\eta_{\mathrm{E}} - \eta_{\mathrm{SE}}) - 4V_{\mathrm{S}}\right]}{D_{\mathrm{S}}(\eta_{\mathrm{E}} - \eta_{\mathrm{SE}})} \tag{15}$$

Thus, with the help of (4), the differential equation (14) can be evaluated and the main-reflector surface (13) can be described in terms of θ_{F}. To conclude, the GO-shaping procedure one should establish the relation between the far-field direction θ – represented by η in (14) – and θ_{F}, together with the condition for $L(\eta_{\mathrm{SE}})$.

Under a GO perspective, the relation between θ and θ_{F} can be obtained by imposing the law of energy conservation to the bundle of rays departing from O and leaving the main reflector after both reflections

$$\int_0^{\theta_{\mathrm{F}}} G_{\mathrm{F}}(\theta'_{\mathrm{F}}) \sin\theta'_{\mathrm{F}}\, \mathrm{d}\theta'_{\mathrm{F}} = N \int_{\theta_1}^{\theta} G_{\mathrm{A}}(\theta') \sin\theta'\, \mathrm{d}\theta' \tag{16}$$

where N is a normalisation factor given by

$$N = \int_0^{\theta_{\mathrm{E}}} G_{\mathrm{F}}(\theta'_{\mathrm{F}}) \sin\theta'_{\mathrm{F}}\, \mathrm{d}\theta'_{\mathrm{F}} \Big/ \int_{\theta_1}^{\theta_2} G_{\mathrm{A}}(\theta') \sin\theta'\, \mathrm{d}\theta' \tag{17}$$

$G_{\mathrm{F}}(\theta_{\mathrm{F}})$ is the circularly symmetric power pattern of the feed, $G_{\mathrm{A}}(\theta)$ is the desired omnidirectional power pattern of the OADE antenna and $\theta = \theta_1$ and θ_2 are the far-field directions corresponding to $\theta_{\mathrm{F}} = 0$ and θ_{E}, respectively. For the ray structures depicted in Figs. 2*a* and 2*b*, $\theta_1 > \theta_2$ and $\theta_1 < \theta_2$, respectively. Notice that the parameters in (16) and (17) and the ray structure must be specified a priori.

The numerical evaluation of (14) determines $L(\eta_{\mathrm{S}})$ to within a constant of scale, i.e. an infinite set of main reflectors, differing from each other by a scale factor, provide the same far-field pattern $G_{\mathrm{A}}(\theta)$, under a GO perspective. To uniquely determine the main reflector, the present shaping procedure assumes a fixed location for P_2 given by the input parameters D_{B} and z_{B} (see Fig. 1). Thus, the condition for $L(\eta_{\mathrm{SE}})$ is determined, with the help of (13), by

$$\vec{r}_{\mathrm{M}}(\theta_{\mathrm{SE}}) = \left[\rho_P + 2\eta_{\mathrm{SE}} e^{L(\eta_{\mathrm{SE}})}\right]\hat{\rho} + \left[z_P + (\eta_{\mathrm{SE}}^2 - 1)e^{L(\eta_{\mathrm{SE}})}\right]\hat{z} = (D_{\mathrm{B}}/2)\,\hat{\rho} + z_{\mathrm{B}}\hat{z} \tag{18}$$

From (18) one obtains

$$L(\eta_{\mathrm{SE}}) = \ln\left(\frac{D_{\mathrm{B}} - 2\rho_P}{4\eta_{\mathrm{SE}}}\right) = \ln\left(\frac{z_{\mathrm{B}} - z_P}{\eta_{\mathrm{SE}}^2 - 1}\right) \tag{19}$$

which helps to determine the scale constant of $L(\eta_{\mathrm{S}})$. Finally, for the case studies discussed in the next section, a fourth-order Runge–Kutta method [20] was used to numerically integrate (14).

5 Case studies

To illustrate the synthesis procedure described in the previous sections, two case studies are discussed below, covering both ray structures illustrated in Fig. 2. In order to explore the potentialities of omnidirectional dual-reflector antennas as base-station antennas in point–multipoint radio links, the main reflector was always shaped to generate an omnidirectional radiation pattern with a cosecant square profile $G_{\mathrm{A}}(\theta)$ in the elevation plane, given by [21]

$$G_{\mathrm{A}}(\theta) = G_{\mathrm{O}} \csc^2(\theta - \pi/2), \quad \text{for} \quad \theta \in [\theta_1, \theta_2] \tag{20}$$

where G_O is a normalisation factor that can be set equal to

$$G_{\mathrm{O}} = \frac{1}{2\pi}\left|\frac{\cos\,\theta_1 \cos\,\theta_2}{\cos\,\theta_1 - \cos\,\theta_2}\right| \tag{21}$$

for unity radiated power. The cosecant square pattern (20) provides a uniform coverage of ground around the antenna [21]. Depending on the main-reflector dimensions, the limiting angles $\theta = \theta_1$ and θ_2 (see Fig. 2) should be specified according to environmental constraints and to minimise interference in adjacent radio links.

The TEM coaxial horn feed used is illustrated in Fig. 3. The feed provides an OADE with a vertically polarised (i.e. θ-polarised) radiated field. To minimise the direct radiation of the feed over the main reflector, an annular $\lambda/4$ choke was placed between the horn's aperture and the main-reflector inner rim [10], as illustrated in Figs. 3, 4, 6 and 8. For GO main-reflector shaping, the feed circularly symmetric radiation pattern was modelled as [7]

$$G_{\mathrm{F}}(\theta_{\mathrm{F}}) = G_{\mathrm{FO}}\left[\frac{J_0(kr_{\mathrm{i}}\,\sin\,\theta_{\mathrm{F}}) - J_0(kr_{\mathrm{e}}\,\sin\,\theta_{\mathrm{F}})}{\sin\,\theta_{\mathrm{F}}}\right]^2, \quad \text{for}\ \ \theta_{\mathrm{F}} \le \pi/2 \tag{22}$$

where G_{FO} is a normalisation factor. Equation (25) represents the radiation from a coaxial aperture mounted on a perfect electric conductor plane, with internal and external radii r_{i} and r_{e}, respectively. In all case studies to be presented, $r_{\mathrm{i}} = 0.45\lambda$ and $r_{\mathrm{e}} = 0.9\lambda$. As the horn aperture dimensions are electrically small, the feed phase centre is practically at the horn's aperture plane.

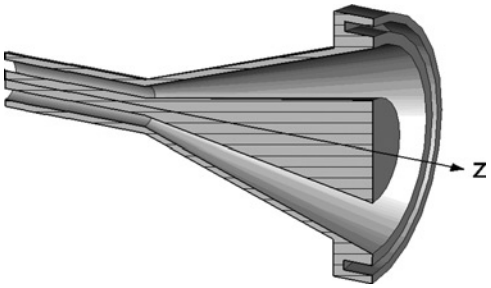

Figure 3 *TEM feed horn geometry*

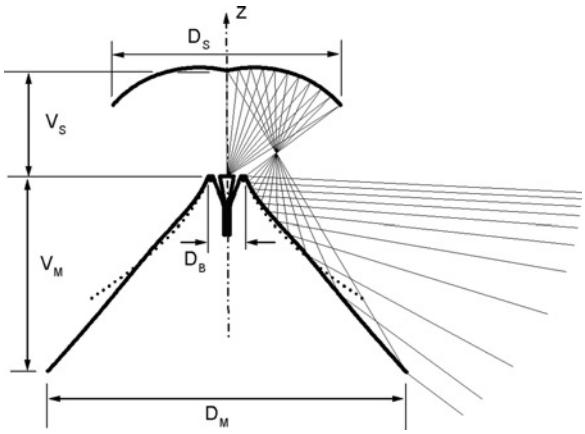

Figure 4 *Sub- and main-reflector generatrices of the shaped OADE antenna of Case I. Main reflector of the classical configuration in dotted lines*

For comparison purposes, the classical OADE configuration described in [14] is used as a reference. In [14] the antennas were designed to provide a main beam tilted 12° away from the horizon with input parameters $z_{\mathrm{B}} = 0$ and $D_{\mathrm{B}} = 2.4\lambda$, providing enough space to accommodate the horn's structure. The subreflector parameters $D_{\mathrm{S}} = 14.71\lambda$ and $V_{\mathrm{S}} = 7.636\lambda$ were established to attain the desired main-beam tilt $\theta = 102°$ (i.e. 12° below horizon), together with a subreflector edge angle $\theta_{\mathrm{E}} = 55°$. The values of the main-reflector projected diameter $D_{\mathrm{M}} = 17.56\lambda$ and of the conical aperture width $W_{\mathrm{A}} = 7\lambda$ were also specified, according to the design procedure for classical configurations [14]. This aperture width W_{A} provided half-power beam widths with ~10°. The subreflector of this classical configuration was used in the first case study discussed below.

5.1 Case I

As a first example (Case I) to illustrate the synthesis, the main reflector was shaped to produce the cosecant square pattern (20) between $\theta_2 = 93°$ and $\theta_1 = 135°$ with a virtual main-reflector caustic, as illustrated in Fig. 2*a*. With the input parameters (D_{S}, V_{S}, D_{B}, z_{B} and θ_{E}) described in the previous paragraph, the conic (ellipse) parameters of the subreflector $\varepsilon = 0.250$, $2c = 3.60\lambda$ and $\beta = 62.4°$ were obtained from (5), (9) and (10). These parameters provided the condition $L(\eta_{SE}) = 0.758\lambda$ from (19). Fig. 4 illustrates the generatrices of the sub- and main reflectors, as well as the main-reflector parabola of the reference classical configuration [14]. The values of relevant dimensions are summarised in Table 1, V_{M} being the distance from P_1 to the origin along the z-axis (see Fig. 2).

For Case I, the increase of the shaped main-reflector dimensions D_{M} and V_{M} observed in Fig. 4 is imposed by the ray arising from the subreflector vertex Q. For large values of θ_1, this ray impinges upon the main reflector at an almost grazing incidence, pushing the edge P_1 downwards. From Fig. 2*a* one observes that the limiting value for grazing incidence is $\theta_1 = \theta_{\mathrm{S0}}$, given by (15). Another consequence of this almost grazing incidence at P_1 is the expectedly high inaccuracy of the GO-based shaping at that region. As the GO-based synthesis does not take into account diffraction and coupling effects among the feed and reflectors, a full-wave analysis based on the MoM technique was conducted to validate the shaping procedure [16–18]. The radiation pattern of the shaped Case I antenna is illustrated in Fig. 5, together with the cosecant square pattern and its ±3 dB limits.

The behaviour of the radiation pattern of Fig. 5 can be understood as follows: from Fig. 4 one observes that the

doi: 10.1049/iet-map.2008.0171

Table 1 Relevant dimensions of the classical [8] and shaped OADE antennas

OADE parameters	Classical configuration	Case I	Case II	Case IIA
D_S (λ)	14.71	14.71	14.71	14.71
V_S (λ)	7.636	7.636	7.636	7.54
θ_E	55°	55°	55°	55°
$z_B(\lambda)$	0	0	0	−0.5
$D_M(\lambda)$	17.56	23.21	16.67	17.8
$V_M(\lambda)$	8.39	14.08	7.95	8.55

upper portion of the main-reflector generatrix resembles a parabola, focusing the beam and, consequently, defining the peak of the radiation pattern. On the other side, the larger main-reflector lower portion spreads the reflected energy, defining the cosecant square pattern observed in Fig. 5. As the quasi-parabolic upper portion is electrically small (corresponding to a height of about 3λ, according to Fig. 4), the half-power beam width of the radiation pattern is relatively large (about 15°, from Fig. 5) with a smooth roll-off above horizon. It would require a main reflector with a larger quasi-parabolic upper portion to focus the beam along the direction $\theta_2 = 93°$ and increase the roll-off above horizon, in order to reduce interference with adjacent cells. However, as one can observe from Fig. 4, the main-reflector upper portion is closer to the ellipse focus. Thus, when ray tubes emerging from the subreflector with the same angular width are compared, that on the top intercepts a smaller segment of the main-reflector generatrix than that at the bottom. This poses a major limitation to the synthesis with a virtual caustic (i.e. $\theta_1 > \theta_2$), as the demand for a main reflector with a larger parabolic upper portion lead to a considerable increase in

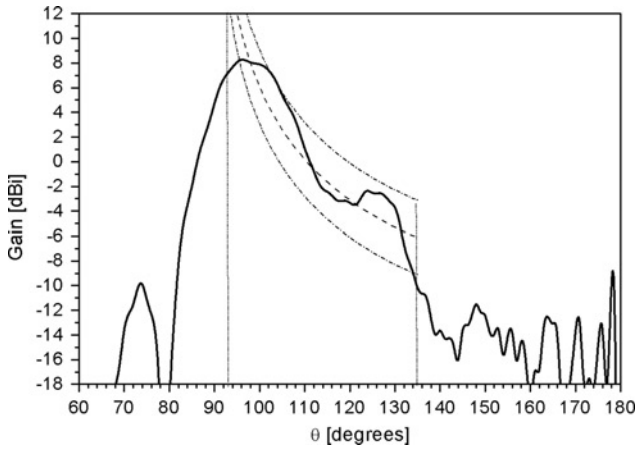

Figure 5 *MoM radiation pattern in the elevation plane of the shaped OADE antenna of Case I (solid line), together with the cosecant square pattern (dashed line) and its ±3 dB limits (dashed-dotted lines)*

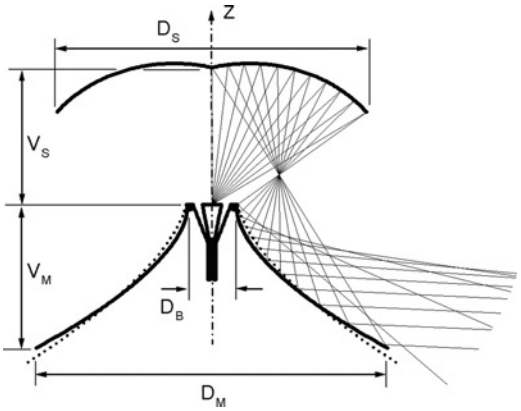

Figure 6 *Sub- and main-reflector generatrices of the shaped OADE antenna of Case II. Main reflector of the classical configuration in dotted lines*

the reflector dimensions and, consequently, the antenna volume.

5.2 Case II

The shaped OADE antenna of the second example (Case II) was designed to radiate (under a GO perspective) the same pattern of Case I, but with a real main-reflector caustic, as illustrated in Fig. 2*b*. Thus, all input parameters and, consequently, the subreflector remain unaltered, except that now $\theta_1 = 93°$ and $\theta_2 = 135°$. The antenna geometry of Case II is depicted in Fig. 6, together with the main-reflector parabola of the reference classical configuration [14]. From Figs. 4 and 6 one observes what is probably the most important feature of the present configuration for the present scenario: Case II main-reflector dimensions D_M and V_M, and, consequently, the overall antenna volumes are considerably smaller than those of Case I. The most relevant dimensions of the shaped antenna are summarised in Table 1.

For OADE configurations with a real main-reflector caustic, like Case II depicted in Fig. 6, it is important to check the shaped main-reflector geometry afterwards, especially when $\theta_2 > \pi - \theta_E$, as the reflector tends to bend towards the space reserved for the feed horn in the region close to point P_2 (see Fig. 6). If necessary, this potential drawback may be compensated by slightly increasing D_B to provide more space for the feed structure. On the other side, as θ_2 increases, especially for $\theta_2 > \tan^{-1}[(D_B - D_M)/(2V_M)]$, the real main-reflector caustic moves towards the main-reflector surface and its edge P_1 may end up blocking some of the rays reflected by the surface region close to P_2, leaving part of the coverage area in the shadow (according to GO principles). A MoM analysis was conducted to validate the shaping procedure for Case II and the radiation pattern in the elevation plane is depicted in Fig. 7, together with the cosecant square pattern of (20) and its ±3 dB limits.

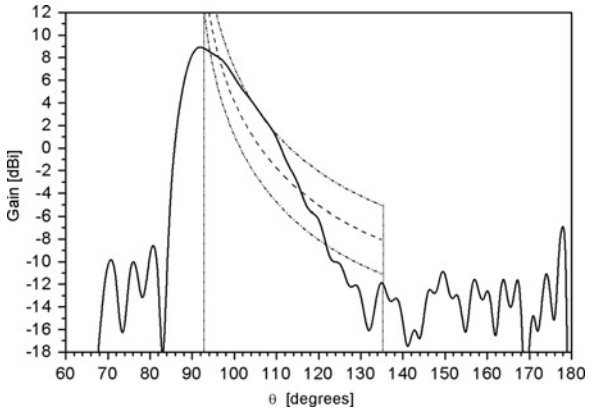

Figure 7 *MoM radiation pattern in the elevation plane of the shaped OADE antenna of Case II (solid line), together with the cosecant square pattern (dashed line) and its ±3 dB limits (dashed-dotted lines)*

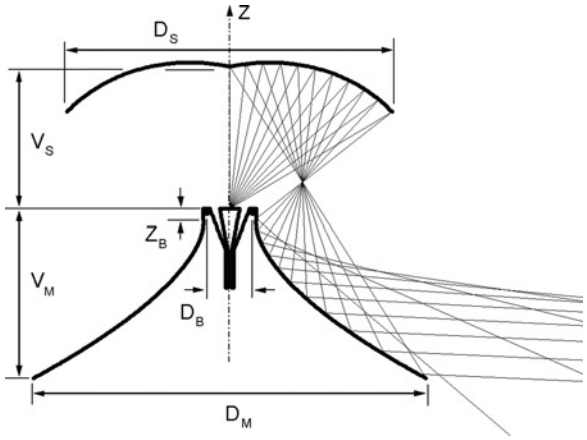

Figure 8 *Sub- and main-reflector generatrices of the shaped OADE antenna of Case IIA*

Because of the finite sizes of the reflectors, one should expect difficulties in achieving the cosecant square pattern (20). However, an unexpectedly pronounced decrease in the radiation pattern for $\theta > 120^\circ$ is observed in Fig. 7. Several MoM analyses of the feed horn and sub- and main reflectors, alone and combined, were conducted to single out the origins of such a pattern behaviour. Although a $\lambda/4$ choke is placed between the feed and the main reflector, the numerical analyses suggest that the electric currents induced near the main-reflector rim P_2 are significantly affected by the coupling between the feed and the main reflector, a phenomenon not accounted for by the GO-shaping procedure. This becomes particularly critical because the small region on the top of the main reflector is responsible for generating the cosecant square pattern, as one can observe from the ray structure depicted in Fig. 6.

To minimise this effect, an alternative shaped OADE antenna was designed, still with a real main-reflector caustic (Case IIA). In order to slightly increase the distance between the horn's aperture and P_2, we have set $z_B = -0.5\lambda$, which alters the subreflector geometry. Thus, we have also adjusted $V_S = 7.54\lambda$ only to generate a main reflector with about the same dimensions of Case II. The other input parameters (D_S, D_B and θ_E) remained the same. The ellipse parameters of the subreflector, obtained from (5), (9) and (10), are $\varepsilon = 0.248$, $2c = 3.59\lambda$ and $\beta = 66.6^\circ$. The corresponding classical main reflector was ignored, but one should expect it to be quite similar to that of the previous classical configuration, as only z_B and V_S were slightly changed. The Case IIA shaped OADE configuration is shown in Fig. 8, with the corresponding ray structure and the dimensions listed in Table 1. Fig. 9 presents the MoM radiation pattern of the antenna, from which one observes that the displacement ($z_B = -0.5\lambda$) between the horn's aperture plane and the main-reflector rim P_2 was effective in minimising the effects of the direct feed radiation on the main-reflector-induced currents.

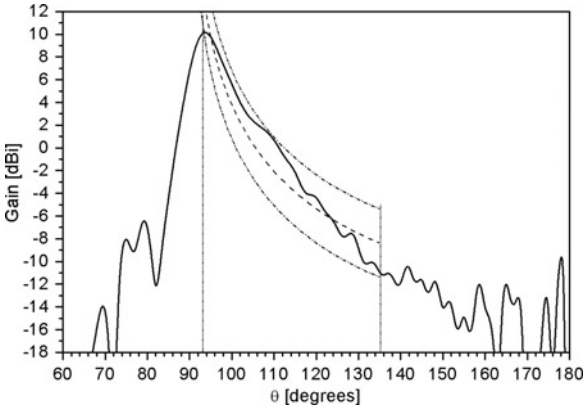

Figure 9 *MoM radiation pattern in the elevation plane of the shaped OADE antenna of Case IIA (solid line), together with the cosecant square pattern (dashed line) and its ±3 dB limits (dashed-dotted lines)*

6 Conclusions

Based on GO principles, a shaping procedure for omnidirectional dual-reflector antennas was presented. The OADE dual-reflector configuration uses an axis-displaced ellipse as a subreflector and a GO-shaped main reflector to control the radiation pattern in the elevation plane. The performance of the proposed GO-shaping procedure was demonstrated on two different reflector configurations that differ by the ray structure that emerges from the main reflector and is directed towards the far-field region. Two cases were synthesised and their performances were verified using accurate MoM analyses. Both cases generate a cosecant squared radiation pattern in the vertical plane and they differ from each other by a real or a virtual main-reflector caustic. For each case, the far-field and geometrical limitations are outlined, such as the limiting value for grazing incidence on the main reflector for rays emerging from the subreflector and the conditions for main-reflector blockage that would leave part of the coverage area in the shadow. It was verified that

doi: 10.1049/iet-map.2008.0171

OADE configurations with real main-reflector caustic can yield relatively compact geometries, together with the desired radiation pattern.

7 Acknowledgments

This work was supported in part by CNPq, Brazil, under Projects 470699/2006-0 and 310945/2006-2, FAPEMIG, Brazil, under Project 4859-6.01/07, CAPES, Brazil, under Project PROCAD 0377058 and by FAPERJ, Brazil, under Project E-26/171083/03.

8 References

[1] PIGGIN P.: 'Emerging mobile WiMax antenna technologies', *Commun. Eng.*, 2006, **4**, (5), pp. 29–33

[2] SEIDEL S.Y.: 'Radio propagation and planning at 28 GHz for local multipoint distribution service (LMDS)'. IEEE Antennas and Propagation Society Int. Symp., Atlanta, USA, June 1998, pp. 622–625

[3] ANDO A., KONDO A., KUBOTA S.: 'A study of radio zone length of dual-polarized omnidirectional antennas mounted on rooftop for personal handy-phone system', *IEEE Trans. Veh. Technol.*, 2008, **57**, (1), pp. 2–10

[4] ZORNOZA J.A., LEBERER R., ENCINAR J.A., MENZEL W.: 'Folded multilayer microstrip reflectarray with shaped pattern', *IEEE Trans. Antennas Propag.*, 2006, **54**, (2), pp. 510–518

[5] MARTÍNEZ-LORENZO J.A., ARIAS M., RUBIÑOS O., GUTIÉRREZ J., GARCÍA-PINO A.: 'A shaped and reconfigurable reflector antenna with sectorial beams for LMDS base station', *IEEE Trans. Antennas Propag.*, 2006, **54**, (4), pp. 1346–1349

[6] NORRIS A.P., WADDOUP W.D.: 'A millimetric wave omnidirectional antenna with prescribed elevation shaping'. Proc. ICAP – 4th Int. Conf. Antennas and Propagation, 1985, pp. 141–145

[7] OREFICE M., PIRINOLI P.: 'Dual reflector antenna with narrow broadside beam for omnidirectional coverage', *Electron. Lett.*, 1993, **29**, (25), pp. 2158–2159

[8] BESSO P., BILLS R., BRACHAT P., VALLAURI R.: 'A millimetric wave omnidirectional antenna with cosecant squared elevation pattern'. Proc. ICAP – 10th Int. Conf. Antennas and Propagation, 1997, pp. 448–451

[9] PINO A.G., ACUÑA A.M.A., LOPEZ J.O.R.: 'An omnidirectional dual-shaped reflector antenna', *Microw. Opt. Tech. Lett.*, 2000, **27**, (5), pp. 371–374

[10] BERGMANN J.R., HASSELMANN F.J.V., BRANCO M.G.C.: 'A single-reflector design for omnidirectional coverage', *Microw. Opt. Tech. Lett.*, 2000, **24**, (6), pp. 426–429

[11] KEZUKA A, KAZAMA Y., YAMADA Y.: 'Antennas with cosecant square radiation pattern both upward and downward for FWA'. IEEE Antennas and Propagation Society Int. Symp., Columbus, USA, June 2003, pp. 782–785

[12] BERGMANN J.R., MOREIRA F.J.S.: 'An omni directional ADE reflector antenna', *Microw. Opt. Tech. Lett.*, 2004, **40**, (3), pp. 250–254

[13] MOREIRA F.J.S., BERGMANN J.R.: 'Classical axis-displaced dual-reflector antennas for omnidirectional coverage', *IEEE Trans. Antennas Propag.*, 2005, **53**, (9), pp. 2799–2808

[14] MOREIRA F.J.S., BERGMANN J.R.: 'Axis-displaced dual-reflector antennas for omnidirectional coverage with arbitrary main-beam direction in the elevation plane', *IEEE Trans. Antennas Propag.*, 2006, **54**, (10), pp. 2854–2861

[15] WESTCOTT B.S., STEVENS F.A., BRICKELL F.: 'GO synthesis of offset dual reflectors', *IEE Proc.*, 1981, **128**, (Pt. H, 1), pp. 11–18

[16] TEIXEIRA F.L., BERGMANN J.R.: 'Moment-method analysis of circularly symmetric reflectors using bandlimited basis functions', *Proc. IEE– Microw. Antennas Propag.*, 1997, **144**, (3), pp. 179–183

[17] OLVER A.D., CLARRICOATS P.J.B., SHAFAI L., KISHK A.A.: 'Microwave horns and feeds' (Electromagnetic Wave Series, IEE Press, 1994)

[18] PETERSON A.F., RAY S.L., MITTRA R.: 'Computational methods for electromagnetics' (Series on Electromagnetic Wave, IEEE Press, 1998)

[19] GALINDO V.: 'Design of dual-reflector antennas with arbitrary phase and amplitude distributions', *IEEE Trans. Antennas Propag.*, 1964, **AP-12**, (4), pp. 403–408

[20] HILDEBRAND F.B.: 'Introduction to numerical analysis' (McGraw-Hill, 1956, 2nd edn.), 1974

[21] CHANG D.C., CHENG Y.C.: 'Development of eight meters inverse cosecant square reflector antenna'. IEEE Antennas and Propagation Society Int. Symp., Orlando, USA, June 1999, pp. 1160–1163